A panchromatic spatially resolved study of the inner 500 pc of NGC 1052 – I. Stellar population

L. G. Dahmer-Hahn [ORCID],[1]★ R. Riffel [ORCID],[1]★ J. E. Steiner,[2] R. A. Riffel [ORCID],[3] R. B. Menezes,[4] T.V. Ricci,[5] N. Z. Dametto,[1] T. Storchi-Bergmann[1] and M. R. Diniz [ORCID][3]

[1]*Departamento de Astronomia, Universidade Federal do Rio Grande do Sul. Av. Bento Goncalves 9500, 91501-970 Porto Alegre, RS, Brazil*
[2]*Instituto de Astronomia, Geofísica e Ciências Atmosféricas, Universidade de São Paulo, 05508-900 São Paulo, Brazil*
[3]*Universidade Federal de Santa Maria, Departamento de Física, Centro de Ciências Naturais e Exatas, 97105-900 Santa Maria, RS, Brazil*
[4]*Centro de Ciências Naturais e Humanas, Universidade Federal do ABC, 09210-580 São Paulo, Brazil*
[5]*Universidade Federal da Fronteira Sul, Campus Cerro Largo, RS 97900-000, Brazil*

ABSTRACT

We map optical and near-infrared (NIR) stellar population properties of the inner 320×535 pc^2 of the elliptical galaxy NGC 1052. The optical and NIR spectra were obtained using the Gemini Integral Field Units of the GMOS instrument and NIFS, respectively. By performing stellar population synthesis in the optical alone, we find that this region of the galaxy is dominated by old ($t > 10$ Gyr) stellar populations. Using the NIR, we find the nucleus to be dominated by old stellar populations, and a circumnuclear ring with younger ($\sim$2.5 Gyr) stars. We also combined the optical and NIR datacubes and performed a panchromatic spatially resolved stellar population synthesis, which resulted in a dominance of older stellar populations, in agreement with optical results. We argue that the technique of combining optical and NIR data might be useful to isolate the contribution of stellar population ages with strong NIR absorption bands. We also derive the stellar kinematics and find that the stellar motions are dominated by a high ($\sim$240 km s^{-1}) velocity dispersion in the nucleus, with stars also rotating around the centre. Lastly, we measure the absorption bands, both in the optical and in the NIR, and find a nuclear drop in their equivalent widths. The favoured explanation for this drop is a featureless continuum emission from the low luminosity active galactic nucleus.

Key words: galaxies: active – galaxies: elliptical and lenticular, cD – galaxies: stellar content.

1 INTRODUCTION

In order to access the stellar population content in galaxies, the technique of stellar population synthesis (e.g. Bica 1988; Cid Fernandes et al. 2004, 2005; Wilkinson et al. 2017) has been widely used over the years, with many key results in galaxy evolution being obtained (Cid Fernandes et al. 2004, 2005; Rembold et al. 2017; Zheng et al. 2017; Goddard et al. 2017a,b; de Amorim et al. 2017; Mallmann et al. 2018). This stellar population synthesis technique has been employed mostly in the optical spectral region. However, with the development of new telescopes focused in other wavelength ranges, it became clear that new evolutionary population synthesis (EPS) models that cover wavelength ranges beyond the optical would have to be developed in order to explore the full potential these telescopes have to offer (Maraston 2005; Riffel et al. 2008; Noël et al. 2013;

Zibetti et al. 2013; Meneses-Goytia et al. 2015; Baldwin et al. 2018; Dahmer-Hahn et al. 2018).

Although the use of near-infrared (NIR) fingerprints on the study of stellar populations started nearly 40 yr ago (Rieke et al. 1980; Origlia, Moorwood & Oliva 1993; Oliva et al. 1995; Engelbracht et al. 1998; Lançon et al. 2001), only in the last decade there was an improvement on the usage of the whole spectral range (Riffel et al. 2008, 2009; Cesetti et al. 2009; Riffel & Storchi-Bergmann 2011; Kotilainen et al. 2012; Storchi-Bergmann et al. 2012; Dametto et al. 2014; Diniz et al. 2017; Riffel et al. 2017). Part of this usage has been due to the lower effect of dust reddening in the NIR, meaning that it is possible to access populations in dustier regions, which in the optical and ultraviolet would be obscured. Also, the most prominent spectral features of stars beyond the main sequence (especially thermally pulsing asymptotic giant branch stars, hereafter TP-AGB stars) are located in the NIR (Maraston 2005; Riffel et al. 2009; Noël et al. 2013; Zibetti et al. 2013; Riffel et al. 2015). Thus, the NIR is crucial in order to identify stellar populations that are dominated by these stars.

★ E-mail: dahmer.hahn@ufrgs.br (LGD-H); riffel@ufrgs.br (RR)
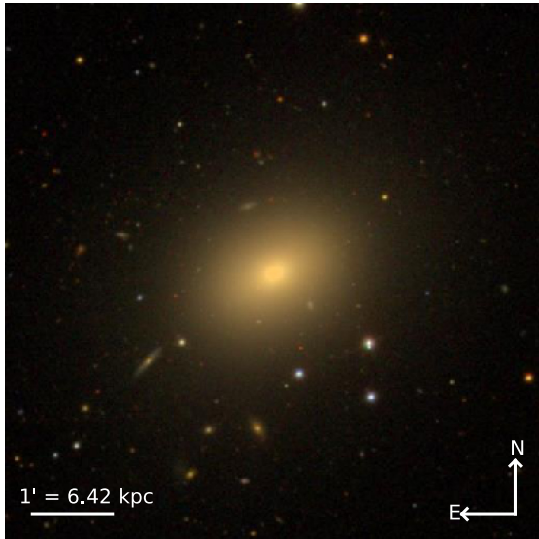
Figure 1. Optical image of NGC 1052 taken with Sloan Digital Sky Survey (Adelman-McCarthy et al. 2006; Baillard et al. 2011).

Two recent papers studied the ability to identify the stellar populations in the NIR compared to the optical region. Baldwin et al. (2018), by studying 12 early-type galaxies, found that the derived star formation histories vary dramatically in the NIR, if compared to the optical, depending on the chosen stellar spectral library. Also, they found that models based on high-quality spectral libraries fit NIR data better and also produce more consistent results when compared to optical ones, with the ages being imprinted on the shape of the continuum in the case of low spectral resolution models. Also, according to Dahmer-Hahn et al. (2018), NIR models with low ($\lesssim 300$) spectral resolution have limitations to distinguish between the different stellar populations, since with these models too much weight is given to the shape of the continuum, when deriving the ages of the stellar populations. Combined, these results show that newer models with higher spectral resolution (e.g. Meneses-Goytia et al. 2015; Röck et al. 2016; Conroy et al. 2018) are essential in order to produce more consistent results in the NIR.

In this work, by using the new library of models of Vazdekis et al. (2016), which has high (~ 2000) spectral resolution both in the optical and in the NIR, we present a study of the stellar population of the nuclear region of NGC 1052 (Fig. 1).

This galaxy is a giant elliptical classified as E4 (Forbes, Georgakakis & Brodie 2001; Xilouris et al. 2004) and with a redshift of 0.005037, harbouring one of the nearest radio-loud active galactic nuclei (AGNs). On radio wavelengths, it displays two jets with slightly different orientations (Wrobel 1984; Fey & Charlot 1997). In X-rays, it shows a compact core, best fitted by an absorbed power law and various jet-related emissions and an extended region (Kadler et al. 2004).

In the optical, its nucleus is classified as low-ionization nuclear emission-line region (LINER, Heckman 1980; Ho et al. 1997). Barth, Filippenko & Moran (1999) used polarized light, and confirmed a hidden broad-line region emission in the H α line, making NGC 1052 the first LINER to have a broad emission component detected in polarized light. Later, Sugai et al. (2005), using integral field spectroscopic data obtained with the Subaru Telescope at a spatial resolution of ~ 0.4 arcsec, reported the detection of weaker features at the nucleus, including the [Fe III] and He II emission lines, as well as an unresolved broad component of the H β emis-

sion. They also found that the spatial structure and velocity field of this source requires the existence of three main components: (i) a high-velocity bipolar outflow, (ii) low-velocity disc rotation, and (iii) a spatially unresolved nuclear component.

Regarding the stellar content of NGC 1052, Raimann et al. (2001) used long-slit spectra and found that the inner 1 kpc is dominated by an older and more metallic stellar population (~ 10 Gyr) whereas a younger, 1 Gyr population becomes increasingly more important outwards. Also, Milone, Rickes & Pastoriza (2007) found, by measuring Lick indices, that the bulge of NGC 1052 is older (12–15 Gyr) and more metallic than the rest of the galaxy, suggesting this galaxy was formed by processes in which the star formation occurred first at the bulge on short time-scales. They also found that, along the major axis, a younger population is responsible for ~ 30 per cent of the light fraction at 1.5 kpc, whereas along the minor axis this stellar population is not important. On the other hand, Pierce et al. (2005) used Keck spectra of 16 globular clusters (GC) and a long-slit spectrum of the whole galaxy, finding that its nucleus has a luminosity-weighted central age of ~ 2 Gyr and [Fe/H] $\sim +0.6$ dex, which is consistent with the merger event that occurred ~ 1 Gyr ago (van Gorkom et al. 1986). They also found that the GCs of NGC 1052 are dominated by an ~ 13 Gyr stellar population, with a few of these GCs having strong blue horizontal branches which cannot be fully accounted for using stellar population models. Based on the age of the GCs, they argued that, despite the recent merger event, little recent star formation occurred.

Also, Fernández-Ontiveros et al. (2011) found 15 compact sources exhibiting H α luminosities an order of magnitude above that estimated for an evolved population of extreme horizontal branch stars. Their H α equivalent widths and optical-to-NIR spectral energy distributions are consistent with them being young stellar clusters with ages < 7 Myr. According to the authors, this is probably related with the merger event experienced by the galaxy.

Regarding the stellar kinematics, Dopita et al. (2015) found that the stars rotate smoothly around the photometric minor axis and are characterized by a velocity dispersion of ~ 200 km s^{-1}. They also found that there is a sharp cusp in the velocity dispersion close to the nucleus, presumably within the zone of influence of the central black hole. These results were later confirmed by Riffel et al. (2017) using NIR data, which also found a centrally peaked σ distribution and a rotation around the photometric minor axis. Besides that, they found an anticorrelation between the h$_3$ momentum and the velocity field, which they interpreted as due to the contribution of stars rotating slower than those in the galaxy disc, probably due to motion in the galaxy bulge.

Most modern libraries of simple stellar populations (SSPs) still lack models younger than 1.0 Gyr in the NIR. This is caused by the low amount of observed hot stars with adequate signal-to-noise ratio and moderate ($R > 1000$) spectral resolution in the NIR. The only library that includes models younger than 1 Gyr is the E-MILES (Vazdekis et al. 2016) library. However, as pointed out by the authors, models younger than 0.5 Gyr are unsafe.

The previous stellar population studies of NGC 1052, which showed that the inner 1 kpc is dominated by stellar populations older than 2 Gyr, make this galaxy an adequate object to have its stellar population properties studied with these modern NIR libraries. Also, while the optical range is more sensitive to bluer stars, the NIR is dominated by the red and cold stars (including the TP-AGB). Combining these two wavelength ranges provides a unique opportunity to test modern stellar population models simultaneously

in the optical and in the NIR. Lastly, because the ionization source of the LINER-like emission in NGC 1052 is still under debate (Fosbury et al. 1978, 1981; Diaz, Terlevich & Pagel 1985; Gabel et al. 2000; Sugai & Malkan 2000; Dopita et al. 2015), combining these two wavelength ranges provides a unique opportunity to search for any contributions of an AGN, since hot dust emission peaks in the NIR and the featureless contribution from the AGN is stronger in bluer wavelengths.

In this work, we aim to study the stellar population properties of NGC 1052, in the optical and NIR separately, and also combining both wavelength ranges in a single fit. This paper is structured as follows: the data and reduction processes are presented in Section 2. In Section 3, we present the method of spectral synthesis used throughout the paper. The results are presented in Section 4, and are discussed in Section 5. Lastly, the conclusions are drawn in Section 6.

2 DATA AND REDUCTION

In order to fully explore the inner region of NGC 1052, we used two sets of datacubes, one in the optical and the other in the NIR. The optical datacube was obtained with Gemini Multi-Object Spectrograph (hereafter GMOS, Hook et al. 2004; Allington-Smith et al. 2002) and the NIR one was obtained with the Near-infrared Integral Field Spectrograph (hereafter NIFS, McGregor et al. 2003), both instruments attached to the Gemini telescopes. Below we describe the observations and data reduction process.

2.1 Optical data

The optical data were obtained on 2013 September 30 as part of GS-2013B-Q-20 Gemini South project using GMOS on integral field unit mode. The original field of view (FoV) is $3\overset{''}{.}5 \times 5\overset{''}{.}0$ ($320 \times 535 \, \mathrm{pc}^2$), with a natural seeing of $0\overset{''}{.}88$, estimated from stars present in the acquisition image, which was taken immediately before the datacube observation. One 30 min exposure was taken, using the B600-G5323 grating, with a central wavelength of 5620 Å. The full width at half-maximum (FWHM) is equal to 1.8 Å throughout the spectra.

The data were reduced using the GEMINI/IRAF package and included: trimming, bias subtraction, bad pixel removal, cosmic ray removal (using the L. A. Cosmic routine van Dokkum 2001), extraction of the spectra, GCAL/twilight flat correction, wavelength calibration, sky subtraction, and flux calibration (taking into account the atmospheric extinction). Finally, the datacube was constructed, with square spatial pixels (spaxels) of $0\overset{''}{.}05$ width.

In order to improve the quality of the data cube, we also applied the following treatment procedures to the data cube: correction of the differential atmospheric refraction, high spatial-frequency components removal with the Butterworth spatial filtering, 'instrumental fingerprint' removal and Richardson–Lucy deconvolution. The final spatial resolution after the data treatment is $0\overset{''}{.}79$, estimated from a spatial profile obtained along the red wing of the broad Hα emission, and the spectral coverage is 4317–6775 Å (Menezes, Steiner & Ricci 2014; Menezes et al. 2015). The optical continuum of the treated datacube is shown on the left-hand panel of Fig. 2.

2.2 Near-infrared data

The NIR data were obtained on 2011 October as part of GN-2010B-Q-25 Gemini North project using NIFS with ALTAIR adaptive optics system. Six 610 s on target exposures were taken in the J
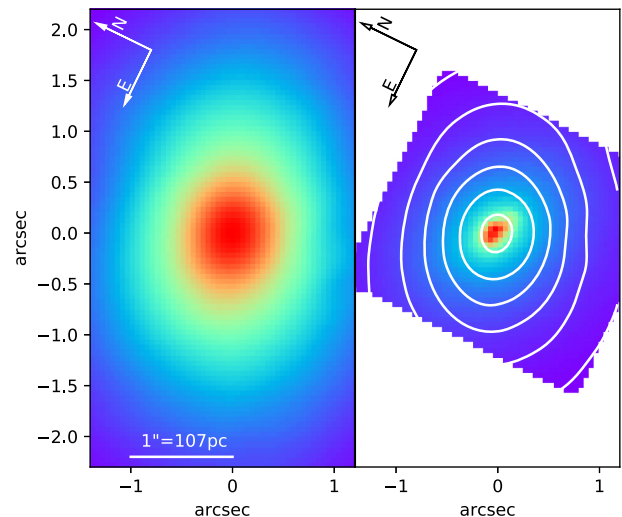

Figure 2. Left-hand panel: optical continuum of NGC 1052 obtained with GMOS. Right-hand panel: NIR *k*-band continuum of NGC 1052 obtained with NIFS. In white are shown optical continuum contours.

band and four 600 s exposures were taken in the *K* band. The spatial resolution is $0\overset{''}{.}1$ and the spectral resolution is 6040 for the *J* band and 5290 for the *K* band.

The data were reduced using the standard reduction scripts offered by the Gemini team, using tasks from the GEMINI/IRAF package. The reduction included trimming of the images, flat fielding, sky subtraction, wavelength and s-distortion calibrations, and telluric absorption removal. The flux calibration was performed by interpolating a blackbody function to the spectrum of the telluric standard star. The reduced datacubes were constructed with square spaxels of $0\overset{''}{.}05 \times 0\overset{''}{.}05$. After the differential atmospheric refraction correction, the individual datacubes in each band were median combined to a single datacube. The combined datacubes were spatially resampled, in order to obtain spaxels of $0\overset{''}{.}021$. This spaxel size was chosen because it is a submultiple value of the original NIFS spaxel dimensions ($0\overset{''}{.}103 \times 0\overset{''}{.}043$). Such spatial resampling provides a better visualization of the contours of the structures. The Butterworth spatial filtering and the instrumental fingerprint removal were then applied. The final spectral coverage of the NIR data is 11472–13461 Å for the *J* band and 21060–24018 Å for the *K* band.

In addition, the original NIFS field of view is $3\overset{''}{.}0 \times 3\overset{''}{.}0$ ($320 \times 320 \, \mathrm{pc}^2$), but due to low signal-to-noise ratio (S/N) on the borders of the FoV, we have shorten it to $2\overset{''}{.}5 \times 2\overset{''}{.}5$. Since *J* and *K* bands were observed on different days, they may present some relative flux calibration problems. In order to minimize these effects, we have compared our data with a cross-dispersed spectrum of NGC 1052 observed with Gemini near-infrared spectrometer (GNIRS) by Mason et al. (2015). This comparison was made using an extraction emulating the GNIRS aperture (slit oriented 90° east of north, with an aperture of $26 \times 155 \, \mathrm{pc}^2$) in our datacubes. After that, we scaled the emulated NIFS long-slit data with the GNIRS ones applying the obtained relation to all single spaxels of our datacube. The GNIRS long-slit spectra, together with the corresponding NIFS extracted spectra of the *J* and *K* bands are shown in Fig. 3. The average correlation of the *J* band was ~80 per cent, whereas for the *K* band it was ~88 per cent. The NIR image of the *K*-band continuum is shown in the right-hand panel of Fig. 2.
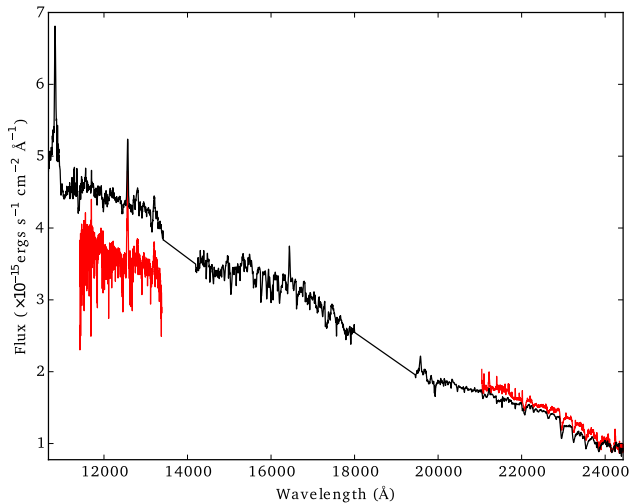
Figure 3. In black, GNIRS long-slit spectra of NGC 1052, as published by Mason et al. (2015). In red, we show the extracted NIFS spectra corresponding to the GNIRS aperture, both in *J* and *K* bands.

2.3 Panchromatic datacube

For an improved characterization of the stellar population of the galaxy, we combined optical and NIR datacubes into a single panchromatic spatially resolved datacube. To do this, we followed the steps below:

(i) First, since the NIR datacube has a higher spatial resolution, we degraded it to match the optical data by convolving it with a Gaussian of FWHM $= 0.7$ arcsec.

(ii) Considering that optical and NIR data were observed on different nights and using different instruments, in order to correct the spectra for scale factors, we extracted an optical spectrum with the same spatial area of the Mason et al. (2015) NIR long-slit spectrum. The spectral separation between the end of the optical datacube and the beginning of the NIR long-slit spectrum is small (<1700Å), so that we searched for the scale factor that yielded the best agreement between the stellar population models and the combined optical + NIR spectrum. We did this by performing spectral synthesis on combined spectra with different scale factors. We found for this step an error ≤ 5 per cent. Lastly, we applied the scale factor to the NIR datacube.

(iii) Assuming that the photometric centre of NGC 1052 in both NIR and optical observations are located at the same position, we sliced each NIR datacube spaxel in 900 subspaxels (30×30) and added their fluxes to the optical spaxel that matched the central position of the NIR subspaxel. This is illustrated in Fig. 4. The combined spectrum of the central spaxel and the spectrum modelled by STARLIGHT are presented in Fig. 5.

This approach of combining optical and NIR data might be useful to identify SSPs which are characterized by bluer colours, such as young populations, as well as stellar populations that are redder, such as intermediate-age ones. Also, since many important stellar features are located in the NIR like the 1.1 µm CN band, the 1.4 µm CN band, and the ZrO features at 0.8–1.0 µm, which are strong indicatives of TP-AGB stars and populations between 0.5 and 2 Gyr (Riffel et al. 2007; Martins et al. 2013; Riffel et al. 2015; Hennig et al. 2018), adding this wavelength range to optical studies can further help to identify the stellar mixture of the galaxy.
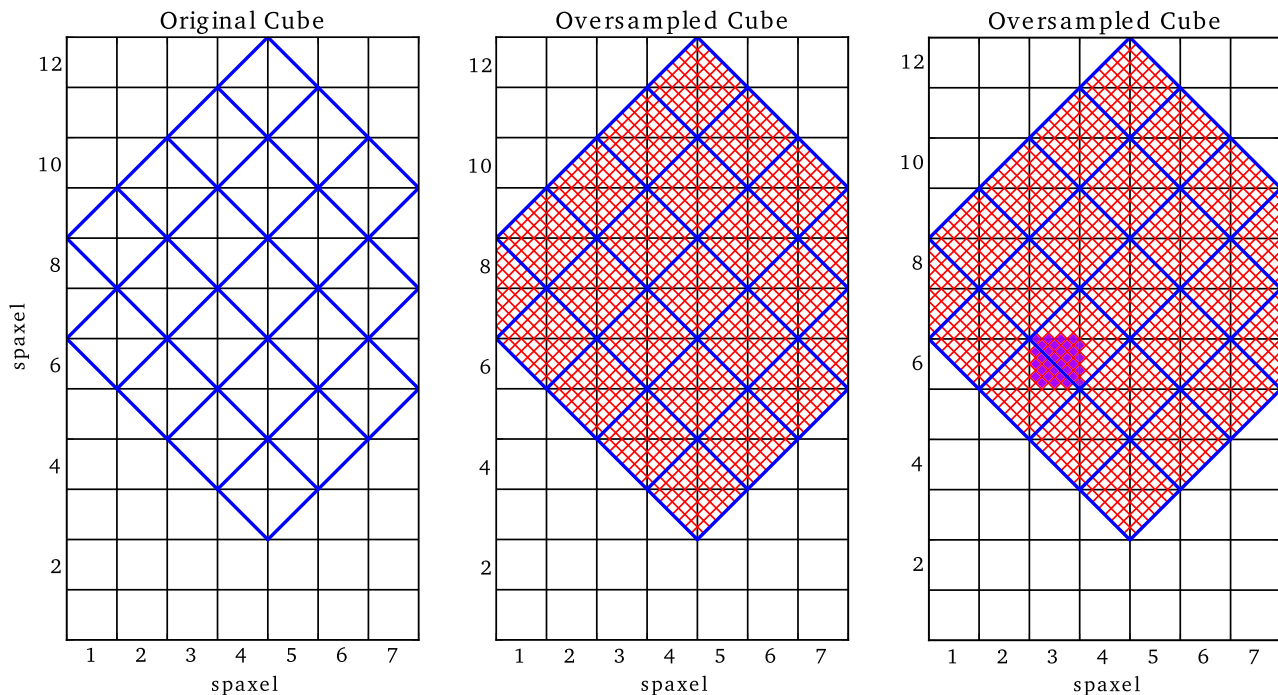
Figure 4. Combination of optical and NIR datacubes. In the left-hand panel, optical data is represented by the black grid and NIR data is represented by the blue grid. In the middle panel, each NIR spaxel was sliced in 64 subspaxels (8×8), represented by the red grid. In our data treatment, we sliced each spaxel in 900 subspaxels (30×30) for better accuracy, rather than the 64 shown in the figure. In the right-hand panel, all subspaxels marked in magenta were added to the optical (3,6) spaxel.
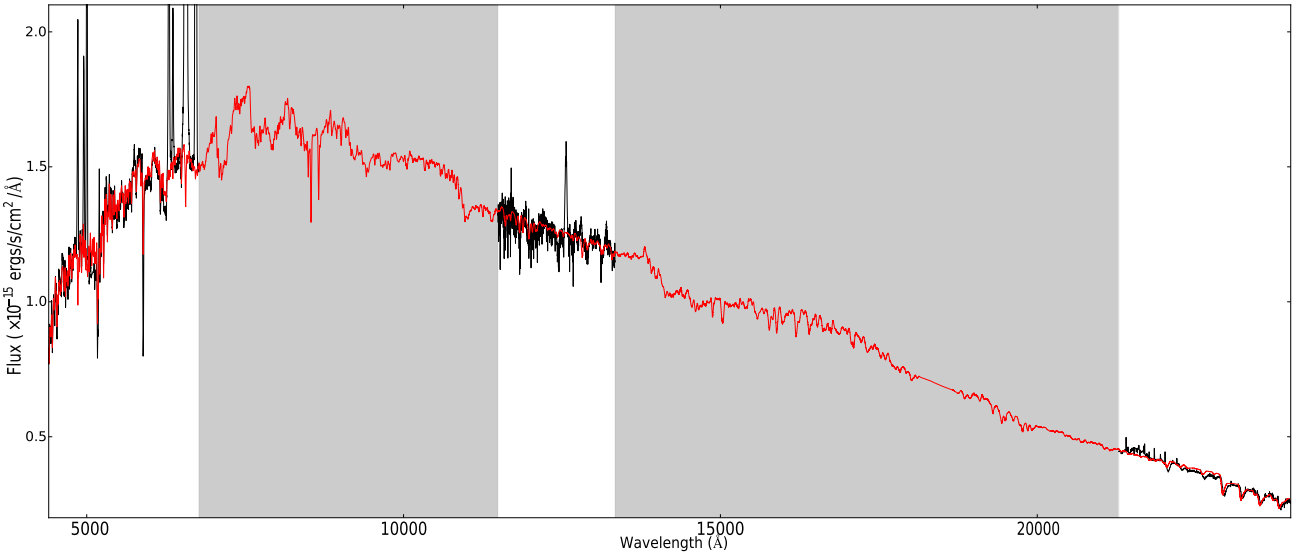
Figure 5. In black, we show the optical and NIR spectra of the combined datacube. Regions where we do not have data are greyed. In red, we present the corresponding spectrum modelled by STARLIGHT with $< t >_L = 10.15$ and $< Z >_L = 0.014$.

3 SPECTRAL SYNTHESIS

To study the stellar population of NGC 1052, we used the STARLIGHT code (Cid Fernandes et al. 2004, 2005, 2013). Basically, the code fits the observed spectrum by a combination of SSPs in different proportions, considering reddening and line-of-sight velocity corrections. The final fit is carried out by STARLIGHT searching for the M_λ model that better describes the data. The model is given by

$$M_\lambda = M_{\lambda 0}[\sum_{j=1}^{N_\star} x_j b_{j,\lambda} r_\lambda] \otimes G(v_\star, \sigma_\star), \qquad (1)$$

where $M_{\lambda 0}$ is the flux at the normalization wavelength $\lambda 0$, $N_\star$ is the number of SSPs used to compose the model, $\vec{x}$ is the population vector so that x_j indicates the contribution from the j-th SSP normalized at $\lambda 0$, $b_{j,\lambda}$ is the j-th model spectrum, r_λ is the reddening term $r_\lambda = 10^{-0.4(A_\lambda - A_{\lambda 0})}$, which is parametrized by the A_V. The stellar velocity dispersions ($\sigma_\star$) and line-of-sight velocities ($v_\star$) are modelled by a Gaussian function $G(v_\star, \sigma_\star)$.

The best fit is carried out by minimizing the equation

$$\chi^2 = \sum_\lambda [(O_\lambda - M_\lambda)w_\lambda]^2, \qquad (2)$$

where O_λ is the observed spectrum. Emission lines and spurious features are masked out by setting $w_\lambda = 0$. Also, because of the lower S/N of the J band, we set $w_\lambda = 0.2$ to the whole wavelength range, both in the NIR and panchromatic synthesis. For the remaining spectral regions, we used $w_\lambda = 1.0$.

To fit the spectra, we used the EPS models developed by Vazdekis et al. (2016, hereafter E-MILES). These models are available with two possible evolutionary tracks and three possible initial mass functions (IMF). We chose the tracks of Girardi et al. (2000) and the Kroupa (2001) IMF, since in the NIR these models are based on the ones published by Röck et al. (2016), which we tested previously (Dahmer-Hahn et al. 2018) and found that they produce self-consistent results.

These models were chosen because they cover the full spectral range of our data (3500–25 000 Å), offering a higher NIR spectral resolution when compared to other stellar population libraries (e.g. Bruzual & Charlot 2003; Maraston 2005; Conroy, Gunn & White

2009). This higher resolution is essential in order to produce better fits of the stellar absorptions.

The only drawback of the E-MILES library is that it used the IRTF library, which does not include hot stars. As a consequence, in the NIR, only SSPs older than 500 Myr are marked as safe by the authors. In the optical region, on the other hand, it includes SSPs as young as 30 Myr. We were then able to test if there are no significant amounts of SSPs younger than 500 Myr.

Also, since NGC 1052 is an elliptical galaxy, we used the reddening law from Cardelli, Clayton & Mathis (1989) to reproduce dust extinction (A_V), which is best suited for objects without active star formation.

In order to remove the noise effects present in real data, a more consistent and robust way to present the stellar population is in the form of condensed population vectors (Cid Fernandes et al. 2004, 2005). Following Riffel et al. (2009), and considering that the library of SSPs only includes models older than 1 Gyr, we defined the light fraction population vectors as follows: xi(1 Gyr $< t \le$ 2 Gyr) and xo(t $>$ 2 Gyr) to represent the intermediate-age and old stellar population vectors, respectively.

Also, to search for a possible emission from the AGN, we followed Riffel et al. (2009) and added to the library of models a featureless continuum with $f_\nu \sim \nu^{-1.5}$. We also added to the NIR library Planck functions with temperatures between 700 and 1400 K in order to reproduce the possible contribution from hot dust.

Lastly, in order to better identify the stellar population mixture of the inner region of the galaxy, we followed Cid Fernandes et al. (2005) and calculated the mean stellar age ($< t >$) and mean metallicity ($< Z >$). They are defined by the following equations:

$$< t >_L = \sum_{j=1}^{N_\star} x_j \log(t_j), \qquad (3)$$

$$< Z >_L = \sum_{j=1}^{N_\star} x_j Z_j, \qquad (4)$$

where t_j and Z_j are the age and metallicity of the j-th SSP. The x_j percentage contribution can be weighted by light (L) and mass (M)

fractions. We normalized optical and panchromatic data at 4500 Å, and NIR data at 21 910 Å. We also used these values to calculate the luminosity contribution. These values were chosen because they contain relatively few stellar absorptions and good S/N.

4 RESULTS

4.1 Stellar synthesis

By fitting the optical datacube with E-MILES library, we found only old stellar content in the entire datacube. Looking at the $< t >_L$, it is possible to see that the cube is dominated by a stellar population of $\sim$12 Gyr, with some locations displaying a slightly younger ($t \sim$ 10 Gyr) stellar population. Also, no contribution from a featureless continuum was found. The A_V throughout the cube was very low ($\sim$0.2 mag), with the nucleus peaking at $A_V = 0.5$ mag. We found metallicity values close to solar ($Z_\odot = 0.019$, Girardi et al. 2000) in the entire cube. We show in the top panels of Fig. 6 the spatial distribution of intermediate-age and old stellar populations, as well as the A_V, $< t >_L$ and Z_L for the optical results.

When fitting the NIR datacube, we found the same results in the nucleus of the galaxy, with a dominance of very old ($t > 10$ Gyr) stellar populations, a higher dust reddening ($\sim$0.8 mag) and solar metallicity. Because of the better spatial resolution of NIR data, the reddening peak is much more concentrated and intense compared to the optical one. Also, no contribution from Planck functions nor from a featureless continuum were found.

However, according to the NIR data, the circumnuclear population is dominated by an $\sim$2.5 Gyr population, which contributes to $\gtrsim$80 per cent of the light. Although this population is classified as old ($t > 2$ Gyr) after binning the results, there is a clear circumnuclear drop in the $< t >_L$ values. The reddening in this region is much lower than the nucleus ($<$0.2 mag), and there is no significant difference in the metallicity if compared to the nucleus. We present these results in the middle panels of Fig. 6.

By performing the synthesis using the panchromatic datacube, we found again a dominance of old stellar populations. No difference in the stellar population can be seen in the $< t >_L$ panel, with the whole panchromatic region displaying an $\sim$10 Gyr stellar population. Also, we found a reddening contribution compatible with both optical and NIR results, as well as a metallicity slightly lower ($Z \sim 0.010$) than solar throughout the datacube. The only exceptions were the borders of the cube, which are affected by a low S/N. As in optical and NIR results, we did not detect contributions from either Planck functions or a featureless continuum. The results for the combined datacube are presented in the bottom panels of Fig. 6.

Since the panchromatic synthesis favoured optical results, we performed the synthesis again, increasing the NIR weight. By setting $w_{NIR} = 2$, the results from STARLIGHT are the same, with a dominance of old stellar populations throughout the cube. When setting $w_{NIR} = 4$, the results found lie in between optical and NIR ones, with a dominance of old stellar populations in the datacube but with $< t >_L \sim$8 Gyr at the borders of the FoV. However, for all fits with $w_{NIR} > 2$, the fits are not able to match the optical spectral region.

4.2 Absorption band measurements

In order to avoid contamination due to stellar kinematics when measuring the equivalent widths (EW) of the absorption bands, we first corrected the spectra for Doppler shift, using the line-of-sight

velocities derived in Section 4.3. We then applied a PYTHON version of the PACCE code (Riffel & Borges Vale 2011) for each spaxel and measured the EWs based on the line limits and continuum bandpasses of Worthey et al. (1994) for the optical region and of Riffel et al. (in preparation) for the NIR, which are presented in Table 1.

From the optical bands, only Feλ5270 Å was not contaminated by emission from the gas and with enough S/N. The NaDλ5895 Å absorption band, although being the strongest in the optical region, was contaminated by the HeIλ5875 Å emission line, as well as by the interstellar sodium. Also, the Mg$_2\lambda$5175 Å band was contaminated by the [N II] λ5198 Å emission line. In the NIR, on the other hand, the three CO bands near 23 000 Å were isolated and with a good S/N ratio ($\sim$100 for the nucleus). The EW maps for the optical FeIλ5270 Å and the three CO bands in the NIR are shown in Fig. 7.

The Fe5270 map shows a constant 2.76 ± 0.17 Å EW throughout the cube, with lower ($\sim$1.8 Å) values closer to the nucleus with a 0″.6 FWHM. The three CO absorptions located in the end of the K band present the exact same spatial distribution, with a constant ($\sim$18 Å) EW throughout the cube and a lower ($\sim$10 Å) EW in the centre. Because of the higher spatial resolution, the EW drop as seen in the NIR is much more concentrated, with an FWHM of 0.26. These results suggest that the component that causes this drop is emitted very close to the nucleus of the galaxy.

4.3 Stellar kinematics

To derive the stellar kinematics, we used the penalized pixel-fitting (pPXF) code, described in Cappellari & Emsellem (2004). Like STARLIGHT, this code also searches for the combination of spectra from a user-provided library to fit the model that better reproduces the observed spectrum. We chose to perform the fitting of the stellar kinematics with pPXF because it allows the user to remove continuum information with a high-order polynomial, so that more weight is given to the stellar features.

In the optical region, we used the Vazdekis et al. (2016) stellar library, since it has an adequate spectral resolution and coverage. For this wavelength range, we fitted the whole cube, masking only the emission lines. For the NIR stellar templates, on the other hand, we used the Winge, Riffel & Storchi-Bergmann (2009) library of late spectral type stellar templates, which was observed with GNIRS, and provides a better spectral resolution ($R > 5000$) and S/N, being limited to the end of the K band ($21\,500 < \lambda < 24\,200$ Å). Since NIR data has a smaller (S/N), especially the K band, we limited the fitting region to 22 830–24 025 Å, where the CO bands are present.

The pPXF code returns as output values for the radial velocity (v_c) and stellar velocity dispersion (σ) for each spatial position. The results are presented in Fig. 8.

In order to search for deviations from circular motions, we followed Bertola et al. (1991) and assumed that the stars are on circular orbits in a plane with a rotation curve given by

$$v_c = \frac{Ar}{(r^2 + c_0^2)^{p/2}}, \tag{5}$$

where A, c_0, and p are parameters to be found and r is the radius. Then, the observed radial velocity at a position (R, Ψ) on the plane of the sky is given by

$$v(R, \Psi) = v_{sys} + \frac{AR\cos(\Psi - \Psi_0)\sin\theta\cos^p\theta}{\{R^2[\sin^2(\Psi - \Psi_0) + \cos^2\Theta\cos^2(\Psi - \Psi_0)] + c_0^2\cos^2\Theta\}^{p/2}}, \tag{6}$$

where Θ is the disc inclination ($\Theta = 0$ being is a face-on disc), Ψ_0 is the position angle of the line of nodes and v_{sys} is systematic velocity of the galaxy. We then developed a script that automatically searches
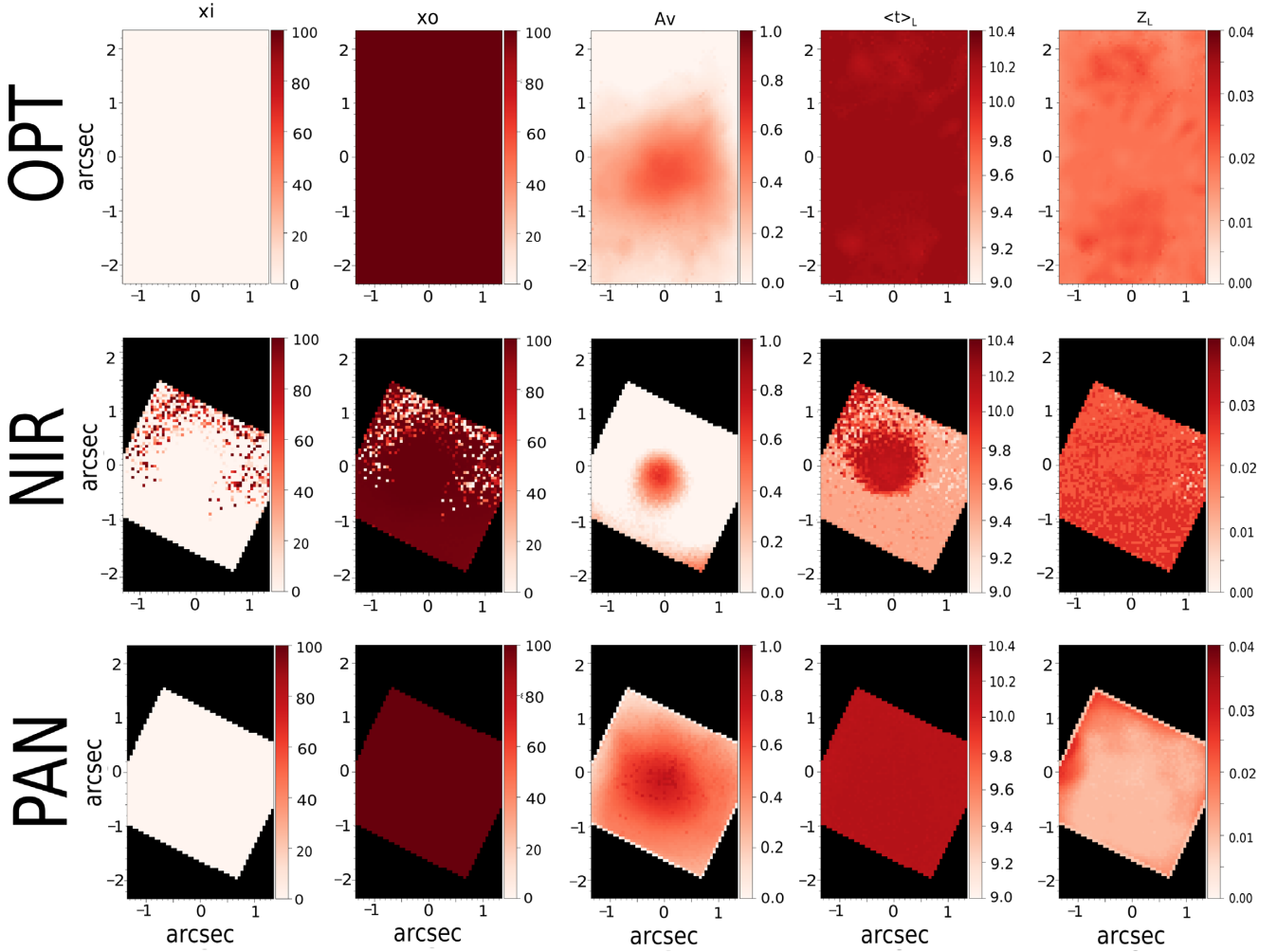
Figure 6. Synthesis results for NGC 1052. From left to right, we present the spatial distribution of intermediate-age and old stellar populations, the A_V, $<t>_L$ and lastly the Z_L. The top five panels show the optical results, the middle panels present the NIR results, and the bottom panels show the results obtained with the combination of optical and NIR data.

Table 1. Line limits and continuum bandpasses.

Centre (Å)	Main Absorber	Line limits (Å)	Continuum bandpass (Å)
5265.65	Fe	5245.650–5285.650	5233.150–5248.150, 5285.650-–5318.150
23 015.0	CO	22 870.000–23 160.000	22 700.000–22 790.000, 23 655.000–23 680.000
23 290.0	CO	23 160.000–23 420.000	22 700.000–22 790.000, 23 655.000–23 680.000
23 535.0	CO	23 420.000–23 650.000	22 700.000–22 790.000, 23 655.000–23 680.000

Note: The optical indices are based on Worthey et al. (1994) and the NIR indexes are based on Riffel et al. (in prep).

for the centre, inclination, and velocity amplitude by performing a Levenberg–Marquardt χ^2 minimization.

Because of the lower S/N of the NIR data, we fitted only the rotation obtained with optical data. In Fig. 9, we present the stellar velocity field, the best-fitting model, and the residual map, obtained by the subtraction of the model from the observed velocities. The residual is, in all locations, below |16| km s^{-1}.

These results show that the stellar motions in the central ∼500 pc of NGC 1052 are dominated by two components: random orbits in the bulge with σ ∼240 km s^{-1} and circular orbits in the galaxy plane with speeds up to 100 km s^{-1}.

5 DISCUSSION

5.1 Divergence in optical and NIR results

The optical results for the stellar population synthesis, revealing that this galaxy is dominated by old stellar content in the nuclear region, are in agreement with past results, which showed that NGC 1052 is dominated by stellar populations older than 2 Gyr (Raimann et al. 2001; Pierce et al. 2005; Milone et al. 2007). Even though one previous paper about this galaxy found spots suggesting younger globular clusters ($t \sim 7$ Myr Fernández-Ontiveros et al. 2011), these
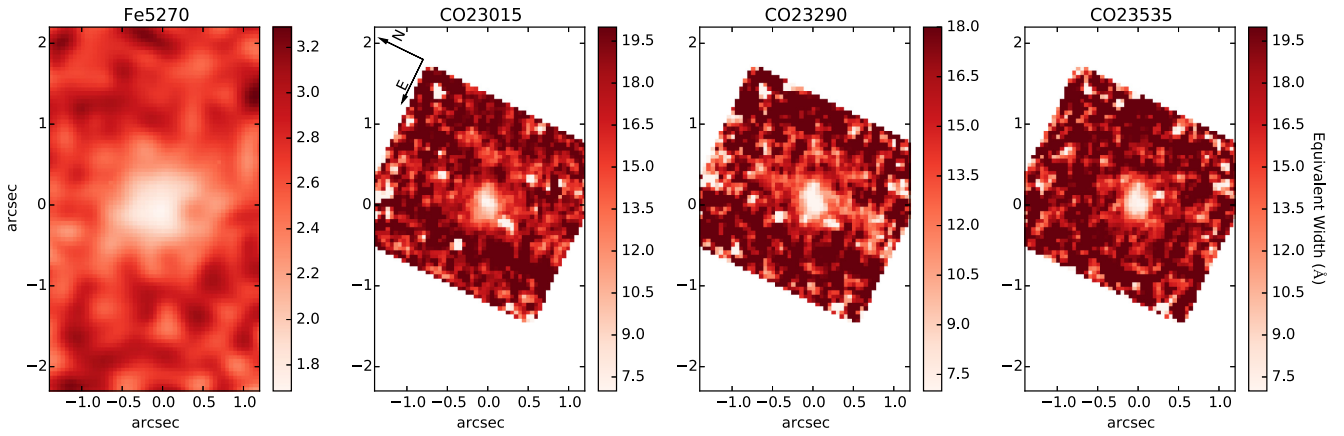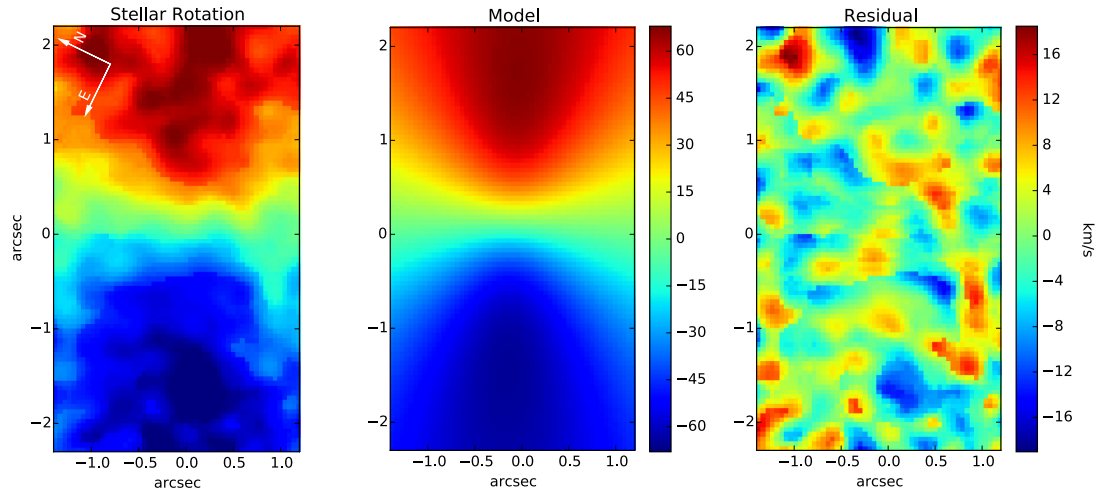
Figure 7. Equivalent width spatial distribution of the optical Feλ5265 Å and the NIR CO bands.
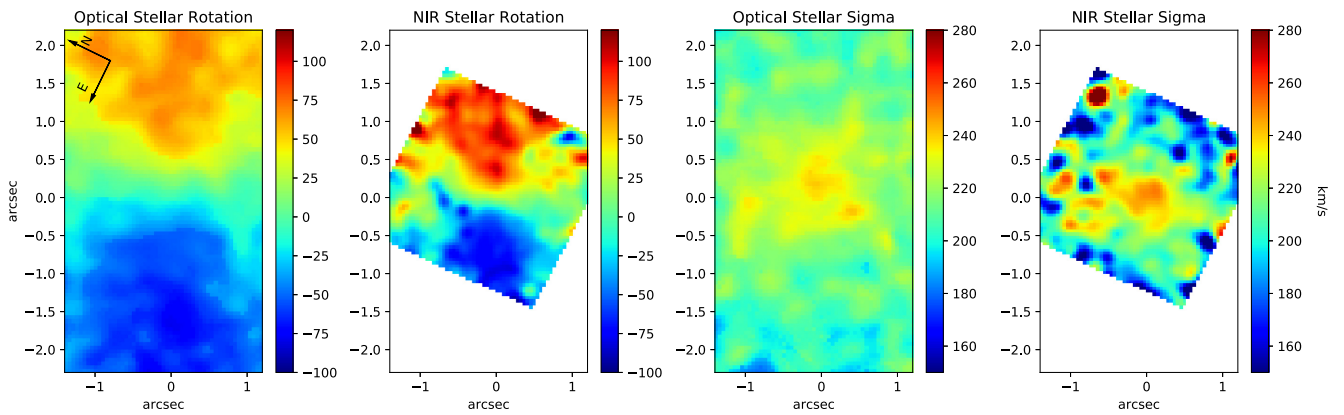
Figure 8. Optical and NIR stellar kinematics derived by pPXF.

Figure 9. Stellar rotation, model, and residual for the optical data.

regions are located outside the FoV of both the optical and NIR datacubes.

On the other hand, NIR results revealed a circumnuclear ring of ∼2.5 Gyr (contributing up to 100 per cent of the light in some regions). This stellar population can be real, in which case NIR data were able to access stellar populations that were not found through optical data. By using NIR data, similar circumnuclear

rings of intermediate-age populations were already reported before (Riffel et al. 2010, 2011; Storchi-Bergmann et al. 2012; Diniz et al. 2017), suggesting that this population can be real. However, the lack of any contribution from stellar populations younger than 10 Gyr in the optical spectra suggests a different explanation, in which these populations are being mistakenly identified by STARLIGHT as a consequence of other factors, discussed below.

5.2 Panchromatic synthesis

The results obtained by combining optical and NIR data favour optical results, with a dominance of old (~ 10 Gyr) stellar populations in the entire FoV. Also, NIR data are well reproduced by the panchromatic fit, suggesting that the result is degenerated. Lastly, our NIR results are in contrast with literature results, which show that elliptical galaxies are dominated by old stellar populations (e.g. Padilla & Strauss 2008; Zhu, Blanton & Moustakas 2010).

Knowing that the intermediate-age circumnuclear ring found in the NIR completely vanished after combining optical and NIR data (which added information allowing the identification of a broader range of stellar populations), our panchromatic results suggest that other factors might me playing an important role in the determination of the stellar population of the NIR data, besides the stellar properties of the galaxy itself. First, we do not have H-band data, which contains more stellar absorptions when compared to J and K bands. Secondly, the low signal-to-noise ratio of the J precludes the presence of enough constraints to STARLIGHT, besides the shape of the continuum. As reported in the literature, the fit of the absorption bands is crucial to the correct determination of the stellar population of the galaxy using NIR data (Baldwin et al. 2018; Dahmer-Hahn et al. 2018). These results combined suggest that the circumnuclear ring found in the NIR might be biased towards younger ages.

Since optical results detected a dominance of old stellar populations, and considering the elliptical nature of NGC 1052, we did not expect to detect a different stellar population by adding NIR data. However, for galaxies dominated by intermediate-age stellar populations, which display unique NIR features (Maraston 2005; Riffel et al. 2007, 2009), this technique of adding NIR data to optical studies might be useful in order to unambiguously determine their stellar populations. This technique might also be useful to study the contents of more luminous AGNs, such as Seyfert galaxies, due to the usual presence of a strong featureless continuum, emitted by the AGN, which peaks in the optical or even bluer wavelengths. The NIR also allows the constraint of the contribution of the AGN hot nuclear torus.

5.3 Equivalent width drop

For the optical Fe5270 index, we compared the EW values with the ones available online for the E-MILES library. For SSPs younger than 1 Gyr, their derived values for this absorption are much smaller than ours, with values close to zero for the younger models and subsolar metallicity. Our off-centre measurements have an average value of 2.76 ± 0.17 Å, and are compatible with a wide range of values. For solar metallicity, the compatible ages range from 2.5 to 6.5 Gyr, whereas for subsolar metallicity the range goes from 1.0 to 4.0 Gyr and for supersolar metallicities range from 6.5 Gyr up to the older models with 14.0 Gyr.

In order to compare NIR absorptions, due to the lack of measurements in the literature, we employed our technique to the E-MILES models and measured their equivalent widths. For the safe models available ($t > 0.5$ Gyr), the EW values range from 14.0 to 18.5 Å for the first CO absorption, 14.4 to 18.8 Å for the second, and 15.4 to 21.1 Å for the third. These measurements are compatible with all our extranuclear measurements for these bands within the standard error of the data (average EW of 17.5 ± 1.2, 17.8 ± 1.0, 20.4 ± 1.1 for the three CO bands, respectively). However, no valuable information can be extracted from these absorptions concerning the stellar population of the galaxy, since nearly all SSPs from 0.5 to 14 Gyr match our data properly.

The spatial distribution of the stellar absorptions shows a nuclear EW drop in the nuclear region, both in the optical and in the NIR, with the same spatial profile of the point spread function of the data. These results suggest that the region in which the EW drop is produced is not spatially resolved, being confined to the region dominated by the LLAGN.

Since the spectral synthesis did not detect any contribution from a featureless continuum or a nuclear variation in the stellar populations, these results indicate that a stellar population synthesis is unable to detect all components that contribute to the emission of this galaxy. It is worth noting that, even the optical synthesis, which was performed with E-MILES library and included both young SSPs and a featureless continuum, did not detect such components.

There are two possible explanations for these EW drops. First, this can be caused by a difference in the stellar population in the central region, such as a young stellar population in which only the hydrogen absorptions are present, and thus could dilute the EWs of the other absorption lines. A second explanation is a featureless continuum caused by the AGN, which can dilute the stellar population features.

Since this galaxy is elliptical, suggesting that high contributions from young populations are not likely to occur, and since it hosts an LLAGN (Wrobel 1984; Fey & Charlot 1997; Kadler et al. 2004; Barth et al. 1999; Sugai et al. 2005), this nuclear EW drop points towards a featureless continuum associated with the LLAGN.

A similar result was already reported by Burtscher et al. (2015), which analysed 51 local AGNs, with NGC 1052 as part of the sample, and found the same EW nuclear drop. They also associated this drop with the contribution from a featureless continuum from the AGN hosted by this galaxy.

5.4 Stellar kinematics

The kinematic results, showing that this galaxy displays a circular rotation and a broadened nuclear dispersion, are in agreement with the ones derived by Dopita et al. (2015) and Riffel et al. (2017). The stellar kinematics of this galaxy is characterized by a rotation with a major axis oriented along the East–West direction (slightly inclined towards Southeast–Northwest) with blueshifted velocities in the eastern region and redshifted velocities in the western region. Also, the stellar sigma peaks at ~ 240 km s^{-1} in the nucleus, with lower (~ 200 km s^{-1}) values closer to the borders. In the NIR, even with a lower S/N, it is possible to see that the rotation pattern agrees with that seen in the optical. The dispersion derived from the NIR data, on the other hand, is ~ 20 km s^{-1} higher if compared to optical values, which is probably a feature caused by the lower S/N of the NIR data.

The stellar sigma peak is cospatial with the EW drop in the absorption lines, suggesting that these two phenomena might be related. The most probable explanation is that both of them are related to the nuclear region, with the sigma peak being also caused by the sphere of influence of the SMBH.

6 CONCLUSIONS

In this work, we studied the spatial distribution of the stellar spectral properties of the inner 320×535 pc^2 of NGC 1052, both in the optical and in the NIR. Our results can be summarized as follows:

The stellar population in the optical is dominated by old ($t > 10$ Gyr) components, with low (~ 0.5) nuclear dust extinction and solar metallicity throughout the galaxy. When performing the synthesis in the NIR, on the other hand, a circumnuclear ring of stellar

populations with ages ∼2.5 Gyr was found, also with low (∼0.8) nuclear dust extinction and solar metallicity throughout the galaxy.

When performing the synthesis in the combined optical and NIR datacube, we found results compatible with the ones found in the optical, with a dominance of old ($t > 10$ Gyr) stellar populations with low (∼0.5) nuclear dust extinction and solar metallicity in the entire FoV.

The absorption bands, both in the optical and in the NIR, display a drop in the equivalent widths in the nucleus. This drop was not detected in the stellar population synthesis, indicating that a stellar population synthesis is unable to identify all components that contribute to the emission of this galaxy. We find that the presence of a featureless continuum emitted by the LLAGN is the most plausible scenario to explain these drops.

Lastly, the stellar kinematics are dominated by two components. Random motions, as shown by the high (∼240 km s^{-1}) velocity dispersion, dominate the nucleus, with the remaining regions dominated by stars rotating in a plane around the centre with speeds up to 100 km s^{-1}.

ACKNOWLEDGEMENTS

REFERENCES

Adelman-McCarthy J. K. et al., 2006, ApJS, 162, 38
Allington-Smith J. et al., 2002, PASP, 114, 892
Baillard A. et al., 2011, A&A, 532, A74
Baldwin C., McDermid R. M., Kuntschner H., Maraston C., Conroy C., 2018, MNRAS, 473, 4698
Barth A. J., Filippenko A. V., Moran E. C., 1999, ApJ, 515, L61
Bertola F., Bettoni D., Danziger J., Sadler E., Sparke L., de Zeeuw T., 1991, ApJ, 373, 369
Bica E., 1988, A&A, 195, 76
Bruzual G., Charlot S., 2003, MNRAS, 344, 1000
Burtscher L. et al., 2015, A&A, 578, A47
Cappellari M., Emsellem E., 2004, PASP, 116, 138
Cardelli J. A., Clayton G. C., Mathis J. S., 1989, ApJ, 345, 245
Cesetti M. et al., 2009, A&A, 497, 41
Cid Fernandes R., Gu Q., Melnick J., Terlevich E., Terlevich R., Kunth D., Rodrigues Lacerda R., Joguet B., 2004, MNRAS, 355, 273
Cid Fernandes R., Mateus A., Sodré L., Stasińska G., Gomes J. M., 2005, MNRAS, 358, 363
Cid Fernandes R. et al., 2013, A&A, 557, A86
Conroy C., Gunn J. E., White M., 2009, ApJ, 699, 486
Conroy C., Villaume A., van Dokkum P. G., Lind K., 2018, ApJ, 854, 139

Dahmer-Hahn L. G., Riffel R., Rodríguez-Ardila A., Martins L. P., Kehrig C., Heckman T. M., Pastoriza M. G., Dametto N. Z., 2018, MNRAS, 476, 4459
Dametto N. Z., Riffel R., Pastoriza M. G., Rodríguez-Ardila A., Hernandez-Jimenez J. A., Carvalho E. A., 2014, MNRAS, 443, 1754
de Amorim A. L. et al., 2017, MNRAS, 471, 3727
Diaz A. I., Terlevich E., Pagel B. E. J., 1985, MNRAS, 214, 41P
Diniz M. R., Riffel R. A., Riffel R., Crenshaw D. M., Storchi-Bergmann T., Fischer T. C., Schmitt H. R., Kraemer S. B., 2017, MNRAS, 469, 3286
Dopita M. A. et al., 2015, ApJ, 801, 42
Engelbracht C. W., Rieke M. J., Rieke G. H., Kelly D. M., Achtermann J. M., 1998, ApJ, 505, 639
Fernández-Ontiveros J. A., López-Sanjuan C., Montes M., Prieto M. A., Acosta-Pulido J. A., 2011, MNRAS, 411, L21
Fey A. L., Charlot P., 1997, ApJS, 111, 95
Forbes D. A., Georgakakis A. E., Brodie J. P., 2001, MNRAS, 325, 1431
Fosbury R. A. E., Mebold U., Goss W. M., Dopita M. A., 1978, MNRAS, 183, 549
Fosbury R. A. E., Snijders M. A. J., Boksenberg A., Penston M. V., 1981, MNRAS, 197, 235
Gabel J. R., Bruhweiler F. C., Crenshaw D. M., Kraemer S. B., Miskey C. L., 2000, ApJ, 532, 883
Girardi L., Bressan A., Bertelli G., Chiosi C., 2000, A&AS, 141, 371
Goddard D. et al., 2017a, MNRAS, 465, 688
Goddard D. et al., 2017b, MNRAS, 466, 4731
Heckman T. M., 1980, A&A, 87, 142
Hennig M. G., Riffel R. A., Dors O. L., Riffel R., Storchi-Bergmann T., Colina L., 2018, MNRAS, 477, 1086
Hook I. M., Jørgensen I., Allington-Smith J. R., Davies R. L., Metcalfe N., Murowinski R. G., Crampton D., 2004, PASP, 116, 425
Ho L. C., Filippenko A. V., Sargent W. L. W., Peng C. Y., 1997, ApJS, 112, 391
Kadler M., Kerp J., Ros E., Falcke H., Pogge R. W., Zensus J. A., 2004, A&A, 420, 467
Kotilainen J. K., Hyvönen T., Reunanen J., Ivanov V. D., 2012, MNRAS, 425, 1057
Kroupa P., 2001, MNRAS, 322, 231
Lançon A., Goldader J. D., Leitherer C., González Delgado R. M., 2001, ApJ, 552, 150
Mallmann N. D. et al., 2018, MNRAS, 478, 5491
Maraston C., 2005, MNRAS, 362, 799
Martins L. P., Rodríguez-Ardila A., Diniz S., Riffel R., de Souza R., 2013, MNRAS, 435, 2861
Mason R. E. et al., 2015, ApJS, 217, 13
McGregor P. J. et al., 2003, in Iye M., Moorwood A. F. M., eds, Proc. SPIE Vol. 4841, Instrument Design and Performance for Optical/Infrared Ground-based Telescopes. SPIE, Bellingham. p. 1581
Meneses-Goytia S., Peletier R. F., Trager S. C., Vazdekis A., 2015, A&A, 582, A97
Menezes R. B., Steiner J. E., Ricci T. V., 2014, MNRAS, 438, 2597
Menezes R. B., da Silva P., Ricci T. V., Steiner J. E., May D., Borges B. W., 2015, MNRAS, 450, 369
Milone A. D. C., Rickes M. G., Pastoriza M. G., 2007, A&A, 469, 89
Noël N. E. D., Greggio L., Renzini A., Carollo C. M., Maraston C., 2013, ApJ, 772, 58
Oliva E., Origlia L., Kotilainen J. K., Moorwood A. F. M., 1995, A&A, 301, 55
Origlia L., Moorwood A. F. M., Oliva E., 1993, A&A, 280, 536
Padilla N. D., Strauss M. A., 2008, MNRAS, 388, 1321
Pierce M., Brodie J. P., Forbes D. A., Beasley M. A., Proctor R., Strader J., 2005, MNRAS, 358, 419
Raimann D., Storchi-Bergmann T., Bica E., Alloin D., 2001, MNRAS, 324, 1087
Rembold S. B. et al., 2017, MNRAS, 472, 4382
Rieke G. H., Lebofsky M. J., Thompson R. I., Low F. J., Tokunaga A. T., 1980, ApJ, 238, 24
Riffel R., Borges Vale T., 2011, Ap&SS, 334, 351

Riffel R., Pastoriza M. G., Rodríguez-Ardila A., Maraston C., 2007, ApJ, 659, L103

Riffel R., Pastoriza M. G., Rodríguez-Ardila A., Maraston C., 2008, MNRAS, 388, 803

Riffel R., Pastoriza M. G., Rodríguez-Ardila A., Bonatto C., 2009, MNRAS, 400, 273

Riffel R., Riffel R. A., Ferrari F., Storchi-Bergmann T., 2011, MNRAS, 416, 493

Riffel R. et al., 2015, MNRAS, 450, 3069

Riffel R. A., Storchi-Bergmann T., 2011, MNRAS, 417, 2752

Riffel R. A., Storchi-Bergmann T., Riffel R., Pastoriza M. G., 2010, ApJ, 713, 469

Riffel R. A., Storchi-Bergmann T., Riffel R., Dahmer-Hahn L. G., Diniz M. R., Schönell A. J., Dametto N. Z., 2017, MNRAS, 470, 992

Röck B., Vazdekis A., Ricciardelli E., Peletier R. F., Knapen J. H., Falcón-Barroso J., 2016, A&A, 589, A73

Storchi-Bergmann T., Riffel R. A., Riffel R., Diniz M. R., Borges Vale T., McGregor P. J., 2012, ApJ, 755, 87

Sugai H., Malkan M. A., 2000, ApJ, 529, 219

Sugai H. et al., 2005, ApJ, 629, 131

van Dokkum P. G., 2001, PASP, 113, 1420

van Gorkom J. H., Knapp G. R., Raimond E., Faber S. M., Gallagher J. S., 1986, AJ, 91, 791

Vazdekis A., Koleva M., Ricciardelli E., Röck B., Falcón-Barroso J., 2016, MNRAS, 463, 3409

Wilkinson D. M., Maraston C., Goddard D., Thomas D., Parikh T., 2017, MNRAS, 472, 4297

Winge C., Riffel R. A., Storchi-Bergmann T., 2009, ApJS, 185, 186

Worthey G., Faber S. M., Gonzalez J. J., Burstein D., 1994, ApJS, 94, 687

Wrobel J. M., 1984, ApJ, 284, 531

Xilouris E. M., Madden S. C., Galliano F., Vigroux L., Sauvage M., 2004, A&A, 416, 41

Zheng Z. et al., 2017, MNRAS, 465, 4572

Zhu G., Blanton M. R., Moustakas J., 2010, ApJ, 722, 491

Zibetti S., Gallazzi A., Charlot S., Pierini D., Pasquali A., 2013, MNRAS, 428, 1479

This paper has been typeset from a TeX/LaTeX file prepared by the author.